JOURNAL OF AIRCRAFT
Vol. 34, No. 1, January–February 1997

Unsteady Fluid Mechanics Applications of Neural Networks

William E. Faller*
Johns Hopkins University, Baltimore, Maryland 21218
and
Scott J. Schreck†
U.S. Air Force Office of Scientific Research, Bolling Air Force Base, Washington, D.C. 20332

The capability to harness or alleviate unsteady aerodynamic forces and moments could dramatically enhance aircraft control during severe maneuvers as well as significantly extend the life span of both helicopter and wind turbine blade/rotor assemblies. Using recursive neural networks, time-dependent models that predict unsteady boundary-layer development, separation, dynamic stall, and dynamic reattachment have been developed. Further, these models of the flow–wing interactions can be used as the foundation upon which to develop adaptive control systems. The present work describes these capabilities for three-dimensional unsteady surface pressures and two-dimensional unsteady shear-stress measurements obtained for harmonic and constant-rate pitch motions. In the near future, it is predicted that such techniques will provide a viable approach for the development of six degree-of-freedom motion simulators for severe vehicle maneuvers as well as a foundation for the active control of unsteady fluid mechanics in a variety of systems.

Nomenclature

C_p = pressure coefficient, $(p - p_\infty)/q_\infty$
c = wing chord length, m
$d\alpha/dt$ = dimensional pitch rate, deg/s
f = frequency, Hz
k = reduced frequency, $c\omega/2U_\infty$
t_{nd} = nondimensional time, tU_∞/c
U_∞ = test section velocity, m/s
α = angle of attack, deg
α^+ = nondimensional pitch rate, $c(d\alpha/dt)\pi/180U_\infty$
ω = $2\pi f$

Introduction

AERODYNAMIC bodies or lifting surfaces subjected to time-dependent unsteady motion histories elicit unsteady boundary-layer behavior, separation, and in severe maneuvers, dynamic stall and dynamic reattachment. For constant-rate pitch-up motions, spanwise nonuniformities in vortex structure, surface pressure topology, and aerodynamic forces have been extensively characterized.[1–4] Surface pressure nonuniformity and time dependency have also been shown for dynamic reattachment on airfoils[5–7] and wings.[8] Experimental studies have documented the commonplace occurrence of unsteady separated flows on wind turbine blades,[9] and dynamic stall effects on the retreating blades of helicopter rotors as well as on straight wings have been extensively summarized.[10,11]

Simplifying the problem by working with a two-dimensional airfoil removes the spanwise effects. However, resolving the details of unsteady boundary-layer growth and separation across a wide range of dynamic conditions remains difficult. For selected two-dimensional cases, unsteady boundary-layer separation has been described both computationally[12] and experimentally.[13,14] The prominent influence of transition on unsteady flowfields for both attached and separated flowfields has been addressed.[14–18]

Nevertheless, neither experimental studies nor computational simulations can provide the capability to characterize three-dimensional unsteady flowfield development across the parameter range likely to be encountered for practical aerodynamic applications. To date, the complex nature of unsteady flowfields has precluded control. However, recent work indicates that, across an extremely broad range of parameters, both steady and unsteady aerodynamics can be modeled using either neural networks or recursive neural networks (RNN).[19–26] Techniques have also been addressed for integrating these unsteady aerodynamic RNN models with mechanical actuators to demonstrate the ease with which adaptive control systems might be produced.[22] Herein, we describe the application of RNNs to the modeling of unsteady boundary-layer development, separation, and dynamic stall.

Methods

Unsteady Surface Pressure Measurement

Unsteady surface pressure measurements were performed in the Frank J. Seiler 0.91 × 0.91 m low-speed wind tunnel located at the U.S. Air Force Academy. A rectangular planform wing (NACA 0015 cross section), having a 15.24-cm chord and 30.48-cm span was bounded at the root by a circular splitter plate 30.48 cm in diameter. Fifteen Endevco 8507-2 miniature pressure transducers were close-coupled to the wing surface through 15 pressure ports located along the chord line. The 15 transducers were located between 0% chord, the leading edge, and 90% chord. These 15 pressure transducers were moved to various spanwise positions. This is shown schematically in Fig. 1a. In all surface-pressure tests, wind-tunnel test section velocity was held constant at 9.14 m/s, corresponding to a chord Reynolds number of 6.9×10^4. Signals originating from the pressure transducers were sampled at 500 Hz per transducer and low-pass filtered at 250 Hz. In all cases, 20 consecutive wing pitch motions were sampled and ensemble-averaged to arrive at the final surface pressure data set for each record. A detailed explanation of the experimental methods has previously been provided.[4,8]

Presented as Paper 95-0529 at the AIAA 33rd Aerospace Sciences Meeting and Exhibit, Reno, NV, Jan. 9–12, 1995; received Dec. 5, 1995; revision received Aug. 15, 1996; accepted for publication Oct. 8, 1996.

*Faculty Research Associate, Department of Mechanical Engineering; currently at David Taylor Model Basin, Code 503, Carderock Division, Naval Surface Warfare Center, Bethesda, MD 20084-5000. E-mail: faller@oasys.dt.navy.mil. Member AIAA.

†Program Manager, Department of Mathematics. Member AIAA.

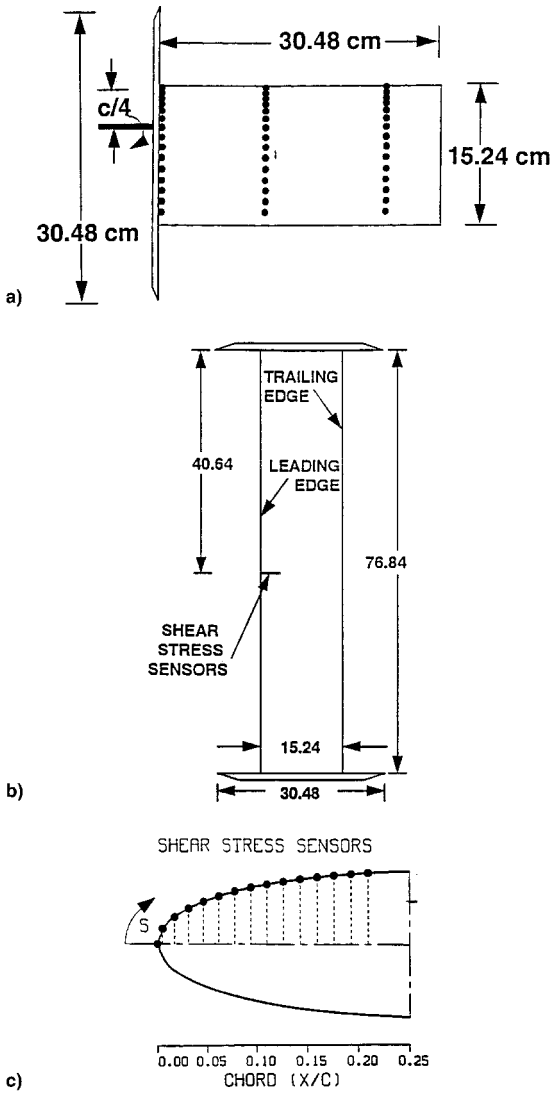

Fig. 1 a) Spanwise and chordwise locations of the pressure transducers for a three-dimensional model, b) planform view of the two-dimensional wing, and c) the locations of the shear-stress elements on a two-dimensional model.

Harmonic Wing Motions

The wing/splitter plate configuration was oscillated sinusoidally in pitch about the wing quarter chord. Three mean angles of attack α_m, three oscillation amplitudes α_ω, and three reduced frequencies k were collected for a total of 27 combinations of α_m, α_ω, and k. The mean angles of attack tested were 5, 10, and 15 deg. The oscillation amplitudes tested were 2, 5, and 10 deg. Reduced frequencies tested were 0.05, 0.10, and 0.15, corresponding to oscillation frequencies of 0.95, 1.9, and 2.86 Hz. For each test condition, one full cycle of data was collected starting and ending at the maximum angle of attack. Note, surface pressure records were collected only at the 37.5% span location for these test conditions.

Following acquisition, the experimental records were divided into two groups. The first group exhibited moving surface pressure minima that indicated the convection of a leading-edge vortex (LEV) (vortex present). This included the nine records with a mean angle of attack of 15 deg and the three records with both a mean angle of attack and oscillation amplitude of 10 deg. The second group did not exhibit surface pressures indicative of a LEV (vortex absent). This group was comprised of all records that did not exceed a maximum angle of attack of 15 deg. This included the nine records with a mean angle of attack of 5 deg and the six records with mean angle of attack of 10 deg and oscillation amplitude of either 2 or 5 deg.

Unsteady Shear-Stress Measurement

Surface shear-stress measurements were performed in the Frank J. Seiler 0.91 × 0.91 m low-speed wind tunnel located at the U.S. Air Force Academy. A two-dimensional airfoil having a NACA 0015 cross section and a 15.24-cm chord was instrumented with a multielement hot-film sensor. Fifteen hot-film sensor elements were located between 0% chord, the leading edge, and 21% chord. The spacing between elements was a uniform 2.54 mm along the upper-surface contour of the airfoil. This is shown schematically in Figs. 1b and 1c. Each element was connected to a constant temperature thermal anemometer having a bandwidth of 10 kHz. A detailed explanation of this type of hot-film array and the experimental measurements has previously been described.[13,14] A detailed explanation of the experimental data pertinent to the model shown herein is available.[14] Briefly, these are uncalibrated shear-stress measurements. Each hot-film sensor has been normalized based on the maximum value recorded per sensor. Thus, the maximum value for each individual hot-film sensor is one. Nevertheless, the time–history of the data is correct, the magnitude is simply uncalibrated.

Starting at 0 deg, the airfoil was pitched up at a constant rate about the wing quarter chord through the static stall angle. Pitch rates $d\alpha/dt$ of 23, 46, 92, 183, 367, and 733 deg/s were employed. Wind-tunnel test section velocities of 3.1, 6.1, 12.2, and 24.4 m/s were tested for each of these pitch rates, corresponding to chord Reynolds numbers of 2.3×10^4, 4.6×10^4, 9.2×10^4, and 1.84×10^5. This yielded nondimensional pitch rates of 0.0025, 0.005, 0.01, 0.02, 0.04, and 0.08 for a test section velocity of 24.38 m/s. Obviously, nondimensional pitch rates are different for other test section velocities. Signals originating from each of the 15 hot-film elements were sampled at 2 kHz and low-pass filtered at 1 kHz. Again, 20 consecutive wing pitch motions were sampled and ensemble-averaged to arrive at the final shear-stress data set for each record. A total of 24 combinations of nondimensional pitch rate and test section velocity were recorded.

RNN Simulations

The RNN architecture is shown schematically in Fig. 2a. A standard sigmoidal activation function, $y = 1/(1 + e^{-x})$, was used for all units. The inputs to the RNN were the unsteady motion history comprised of the instantaneous α, the angular velocity $d\alpha/dt$, the angular acceleration $d^2\alpha/dt^2$, and the surface pressure or shear-stress initial conditions at time t_0. Thus, the input layer was composed of 18 units for the harmonic motion surface pressure model as well as for the shear-stress model (one span location). Similarly, the output layer was composed of 15 units in both cases. In all models, both hidden layers were composed of 32 units. The targeted outputs were either the surface pressure or shear-stress values at time $(t + \Delta t)$. Subsequently, to model the time dependence, the RNN predictions were fed back as inputs to the RNN throughout the motion history. This type of RNN model has previously been described in detail.[22,23]

In all cases, to train the models, a subset of the available data records was used to teach the RNN the relationship between time-dependent motion histories and the temporal evolution of either the unsteady surface pressures or shear stresses. All initial connection weights were set randomly between −0.25 and 0.25. The data sets were presented randomly with the stipulation that each data set be presented an equal number of times. The models were trained using a time-series algorithm based on backpropagation. For all models, training was continued until the time-averaged error was less than 5% for each of the training sets.

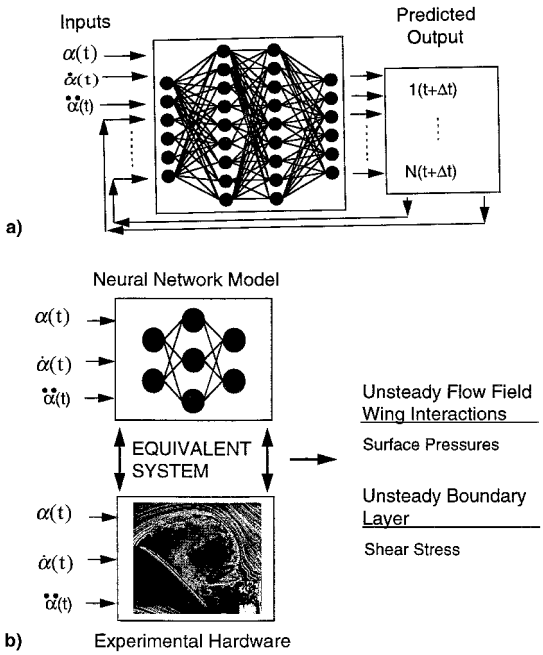

Fig. 2 a) RNN architecture and b) operational RNN following training (fixed weights).

Unsteady Surface Pressure Simulation

For the harmonic motion histories, three different models were developed. One model was trained only on records that did not exhibit evidence of an LEV. In this case, 10 of 15 such vortex absent records were used to train the model. Post-training generalization to other vortex absent records as well as the capability to generalize from vortex absent flow conditions to flow conditions that exhibited a LEV could be addressed. A second model was trained only on vortex present records that exhibited evidence of an LEV. This model was trained on 8 of the 12 available LEV records. Post-training generalization to other LEV records as well as the capability to generalize from vortex present flow conditions to vortex absent flow conditions could be addressed. A third model was trained across the entire parameter space, both types of records were included in the training data. In this case, 18 of the 27 records were used to train the model. Post-training generalization to both record types could be addressed. Overall, these three models provided an opportunity to study RNN performance characteristics and to qualitatively address some of the similarities and differences between vortex absent flowfields and flowfields that were characterized by the presence of an LEV.

Unsteady Shear-Stress Simulation

Unsteady boundary-layer development was modeled using the same RNN paradigm shown schematically in Fig. 2a. For the shear-stress measurements, two different models were developed. One model was trained only on a test section velocity of 24.4 m/s and four of six pitch rates (23, 46, 183, and 733 deg/s). This model was used to determine the capability of RNNs to model time-dependent unsteady boundary-layer behavior. The second model was trained on three of four test section velocities, 12.2 m/s was excluded, and the same four of six pitch rates. This model incorporated the test section velocity as an input, and was used to determine RNN predictive capabilities across a limited range of Reynolds number.

Results

The operational characteristics of the RNN models are shown schematically in Fig. 2b. The only external inputs were the instantaneous α, the angular velocity $d\alpha/dt$, and the angular acceleration $d^2\alpha/dt^2$. For each input motion history the RNN model, in turn, yielded either the time-dependent unsteady surface pressures or unsteady shear stresses. Significantly, the modeled flow–wing interactions generated by any motion history, including harmonic motions and complex ramp histories (composed of multiple pitch rates), can be computed faster than real-time using this approach.

To evaluate the RNN performance, the model-predicted values were compared directly to the experimentally measured data. The performance of the model was verified in two ways, graphically by coplotting the experimentally measured values against the RNN predicted values, and quantitatively by calculating the time-averaged error between the predicted and measured values. Note, all figures, except two (Figs. 6a and 7a), are for records on which the recursive neural network models were not trained. Thus, the capability of RNNs to provide a practical solution to unsteady fluid mechanics problems is clearly demonstrated. Further, the results summarize the complete range of motion histories and flowfield types that have been modeled using RNNs.

Unsteady Surface Pressures

In all figures, time-varying surface pressure at port 1, the leading edge, is at the bottom of the figure. Time-varying surface pressure at port 15, 90% chord, is at the top. The ordinate is surface pressure and the abscissa is nondimensional time. The measured data are shown as solid lines and the RNN predictions as dashed lines. Surface pressure magnitudes are accurate and increase toward the bottom of the figure. Note, the plots have been offset to ease comparison.

Pitch-Up Wing Motions

Figure 3a shows the graphical analyses for a nondimensional pitch rate of 0.15 at the 37.5% span location. This record was not used during training. The RNN accurately models the initial surface pressure decline for the first two port locations. At the remaining port locations, however, the initial surface pressure decline was slightly underpredicted. Although suction peak magnitudes were slightly underpredicted, the model accurately predicted the suction peak time of occurrence for all port locations. Similar results were obtained for the remaining two records corresponding to the wing root and tip. Consistent results were obtained for other constant pitch rates previously unseen by the RNN model. These results have been described in detail.[22] Overall, the results showed that given only limited training data, a single RNN model can be developed that accurately predicts dynamic stall throughout the experimentally bounded parameter space.

Pitch-Down Wing Motions

Figure 3b shows the results for a nondimensional pitch rate of 0.075 at the 37.5% span location. This record was not used during training. The model accurately predicted the initial surface pressure rise. The increase in surface pressure is then followed by a surface pressure decrease. This decrease in surface pressure, which proceeds from the leading-edge region to the trailing edge of the wing, indicates flowfield reattachment. Based on this definition, time of flowfield reattachment was accurately predicted by the model. However, the magnitude of the pressure reversal was underpredicted. Interestingly, the records at 0 and 80% span were predicted more accurately. These results have been described in detail.[23] These results support the previous indication, from dynamic stall models, that highly accurate real-time models of unsteady separated flowfields can be developed using RNNs. Note, because of the relatively small magnitude of the pressure readings, a factor of 5–10 smaller than for dynamic stall, the signal reflects mechanical vibrations in some instances, despite ensemble averaging.

Harmonic Wing Motions

Again, only results for records on which the RNN model was not trained are shown. In all figures, the data record starts and ends with the wing at the maximum angle of attack.

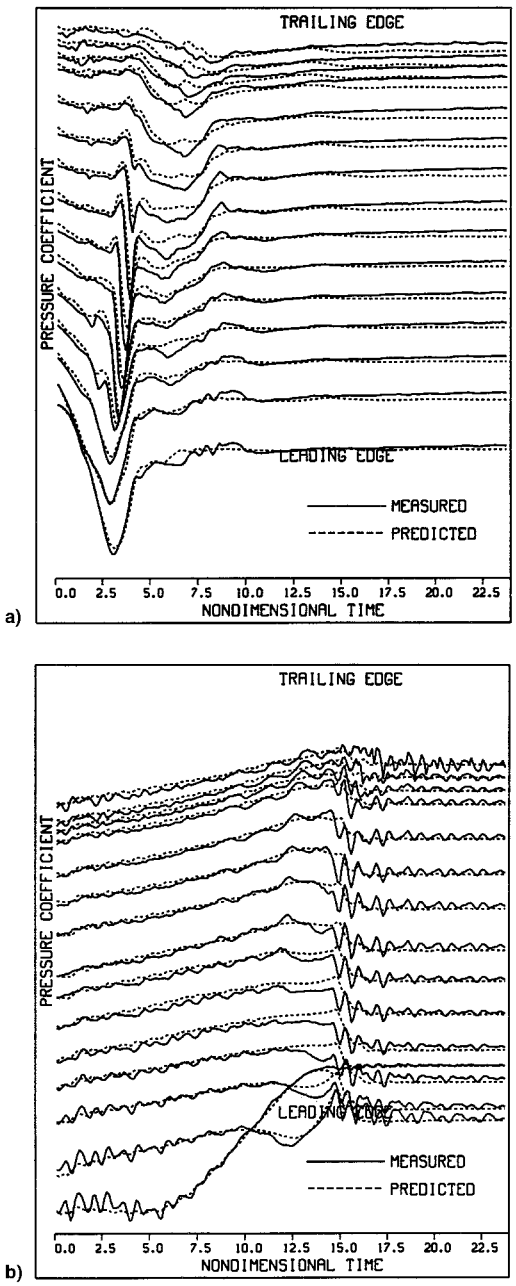

Fig. 3 Predicted and measured surface pressures for a) a pitch-up wing motion ($\alpha^+ = 0.15$ at 37.5% span) and b) a pitch-down wing motion ($\alpha^+ = 0.075$ at 37.5% span).

Figures 4a and 4b show the results for the RNN model trained across the full parameter space (both vortex absent and vortex present records). Figure 4a shows the RNN prediction for a record that exhibited a LEV. Mean angle of attack was 15 deg, oscillation amplitude was 10 deg, and reduced frequency was 0.10. Initial surface pressure magnitudes are underpredicted, followed by a slight overprediction. However, most of the descending and ascending phase of the motion history are accurately modeled, including generation and convection of the LEV. Figure 4b shows the RNN prediction for a record that did not exhibit a LEV. Mean angle of attack was 5 deg, oscillation amplitude was 10 deg and reduced frequency was 0.10. Near the leading edge, initial surface pressure magnitudes are slightly overpredicted. However, both the descending and ascending phase of the motion history were accurately modeled.

In general, as measured by the time-averaged error, the RNN model predicted the surface pressures to within 5% of the experimental data. Consistent results were obtained both for the training data as well as for generalization to other harmonic motions. It is worth noting, however, that the most difficult records to model were those with the smallest oscillation amplitude (2 deg). In these cases, the error was roughly 10%. Nevertheless, these results strongly suggest that a RNN trained on both vortex absent and vortex present flowfield conditions can accurately model the entire parameter space bounded experimentally by the full range of harmonic motion histories tested.

Figures 5a and 5b show the results for the RNN model trained only on records that exhibited an LEV. To maintain consistency, model predictions are compared to the same measured data used in Fig. 4. Figure 5a shows the prediction for the vortex present case. Again, mean angle of attack was 15 deg, oscillation amplitude was 10 deg, and reduced frequency

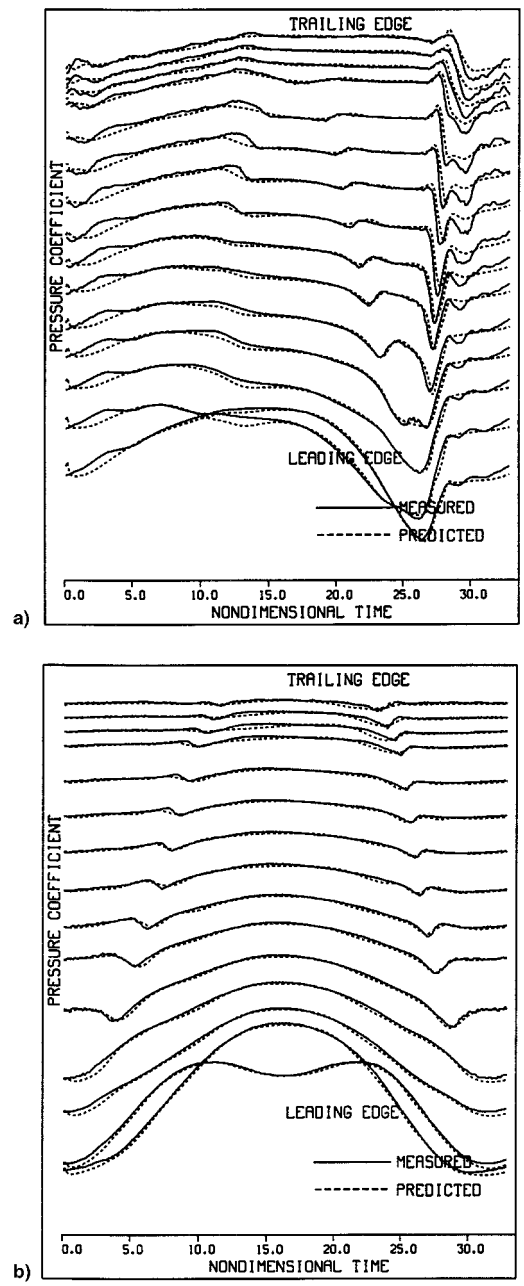

Fig. 4 RNN predictions for model trained on both vortex absent and LEV (vortex present) records. Predicted and measured surface pressures for a harmonic wing motion: a) $\alpha_m = 15$ deg, $\alpha_\omega = 10$ deg, $k = 0.10$ at 37.5% span and b) $\alpha_m = 5$ deg, $\alpha_\omega = 10$ deg, $k = 0.10$ at 37.5% span.

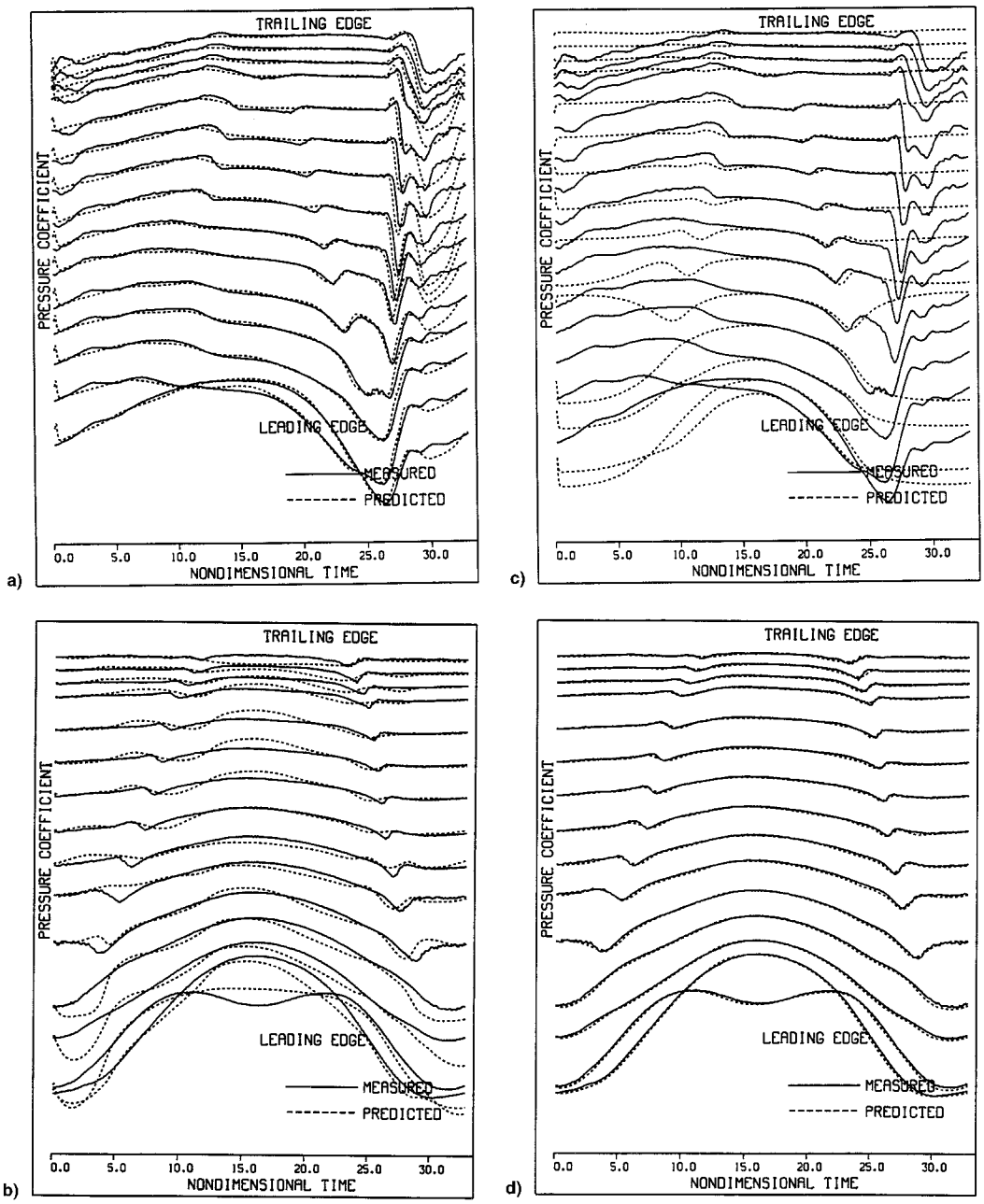

Fig. 5 a) and b) RNN predictions for model trained on only LEV (vortex present) records. c) and d) RNN predictions for model trained on only vortex absent records. a) and c) Predicted and measured surface pressures for a harmonic wing motion (α_m = 15 deg, α_ω = 10 deg, k = 0.10 at 37.5% span). b) and d) Predicted and measured surface pressures for a harmonic wing motion (α_m = 5 deg, α_ω = 10 deg, k = 0.10 at 37.5% span).

was 0.10. For all pressure port locations initial surface pressures are underpredicted, following which constant surface pressure values were accurately predicted. Near the leading edge, the LEV was accurately predicted; however, following convection of the vortex downstream, the surface pressure magnitudes were overpredicted. Similarly, near the trailing edge the LEV is reasonably well predicted; however, the surface pressure magnitudes are substantially overpredicted following vortex passage. Figure 5b shows the prediction for the vortex absent record. Again, mean angle of attack was 5 deg, oscillation amplitude was 10 deg, and reduced frequency was 0.10. Near the leading edge, the initial surface pressure magnitudes are substantially overpredicted. In general, for vortex absent records, the RNN predictions show relatively large errors in both amplitude and phase with respect to the experimental data.

In general, as measured by the time-averaged error, the vortex present RNN model can be characterized as follows. For LEV records, the RNN predicted surface pressures were within 10% of the experimental data. As shown, the model had the most difficulty predicting the surface pressure magnitudes following passage of the LEV. In addition, test cases with the smallest oscillation amplitude (2 deg) also caused increased prediction error. For vortex absent records, the RNN predicted surface pressures yielded errors greater than 10%. Clearly, these results indicate that an RNN model trained only on vortex present flowfield conditions does not accurately model the entire parameter space. Further, just considering predictions of the LEV cases, the results clearly indicate that the model trained on both vortex absent and vortex present records was more accurate than the model trained only on LEV cases.

Figures 5c and 5d show the results for the model trained only on vortex absent records. Again, to maintain consistency, the same two test cases are shown. Figure 5c shows the RNN prediction for the LEV case. For all pressure port locations surface pressure predictions are poor. However, near 0-deg angle of attack, between nondimensional times 15.0–20.0, surface pressure predictions are accurate and flowfield separation during the ascending phase is reasonably well predicted. Clearly, the model does not predict the dynamic stall vortex. Figure 5d shows the RNN prediction for the steady case. Clearly, all predicted surface pressures had less than a 5% error, and flowfield reattachment and separation were accurately predicted in both magnitude and phase.

In general, as measured by the time-averaged error, the vortex absent RNN model can be characterized as follows. For the prediction of LEV (vortex present) records, the model predicted unsteady surface pressures were inaccurate. As shown in Fig. 5c, after a nondimensional time of 25.0, the model does not predict the surface pressures associated with the LEV. For vortex absent records, the RNN-predicted surface pressures were highly accurate (less than 5% error). Again, consistent with results shown earlier, the most difficult cases to model were those with the smallest oscillation amplitude (2 deg). Clearly, these results indicate that a RNN model trained only on vortex absent flowfield conditions does not accurately model the entire parameter space. However, just considering predictions of the vortex absent cases, the results clearly indicate that the model trained only on vortex absent conditions was more accurate than the model that was trained on both types of records.

Overall, the results from all three RNN models suggest the following physical relationships across flowfield conditions.

1) The results indicate that flowfields that do not exhibit a LEV (vortex absent) can be described by a set of physical rules, derived solely from vortex absent records. As such, these rules appear to be independent of the physical rules governing flowfields that do exhibit an LEV. Thus, an RNN model trained only on the vortex absent test cases is extremely accurate throughout that portion of the parameter space, but does not model the dynamic stall vortex.

2) The results indicate that the physical rules governing flowfields that do give rise to an LEV (vortex present) are not determinable solely from vortex present records. The rules appear to be at least partially dependent on the rules that describe the vortex absent cases. Thus, a RNN model trained only on the vortex present test cases accurately predicts the LEV, but yields prediction errors following LEV passage.

3) An RNN trained on both types of records accurately models the entire parameter space bounded experimentally by the full range of harmonic motion histories tested. Whereas, a model trained solely on either type of record does not model the full parameter space. Thus, the results indicate that an accurate set of physical rules describing both vortex absent and vortex present flowfields can best be determined from a mix of both types of records. Since the vortex present RNN model predicts the vortex absent test cases significantly better than the vortex absent model predicts the LEV test cases, this mix seems to be weighted toward the vortex present rules.

Unsteady Shear Stress

In all figures, element 1, the leading edge, is at the bottom of the figure, and element 15, 21% chord, is at the top. The ordinate is normalized output voltage, uncalibrated shear-stress measurements, and the abscissa is nondimensional time. All hot-film sensor voltage values have been normalized to the same maximum value of one. Measured values are shown as a solid line and the RNN predictions as a dashed line. Again, the plots have been offset to ease viewing.

For all elements, increased heat transfer is in the downward direction (toward the bottom of the figure). In all cases, near the leading edge, in response to increasing wing pitch angle, the flow is accelerated and heat transfer initially increases (negative or descending traces). However, for elements farther downstream, increasing wing pitch angle causes a decrease in the heat transfer (positive or ascending traces). This decrease in heat transfer is indicative of boundary-layer thickening. Following boundary-layer thickening, the rapid increase in heat transfer is caused by unsteady boundary-layer transition. Following LEV passage heat transfer again decreases.

Figures 6a and 6b show the results for the RNN model trained on only one test section velocity (24.4 m/s, Reynolds number 1.84×10^5). Figure 6a shows the results for a pitch rate on which the model was trained (46 deg/s). Initial shear-stress values are accurately predicted, except at element 7. Boundary-layer thickening and transition are reasonably well predicted. However, the model predicted values tend to lag the measurements. Following passage of the LEV, the model does not predict the time at which shear stress decreases. Figure 6b

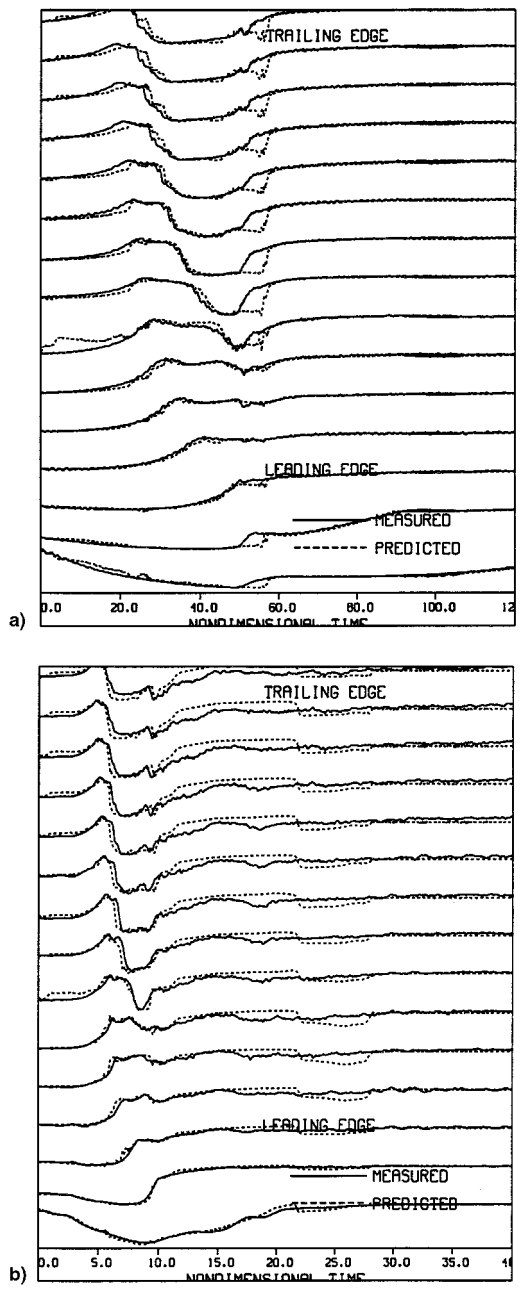

Fig. 6 RNN predictions for a shear-stress model trained on one test section velocity (Reynolds number 1.84×10^5). Predicted and measured shear-stress values for a pitch rate of a) 46 and b) 367 deg/s.

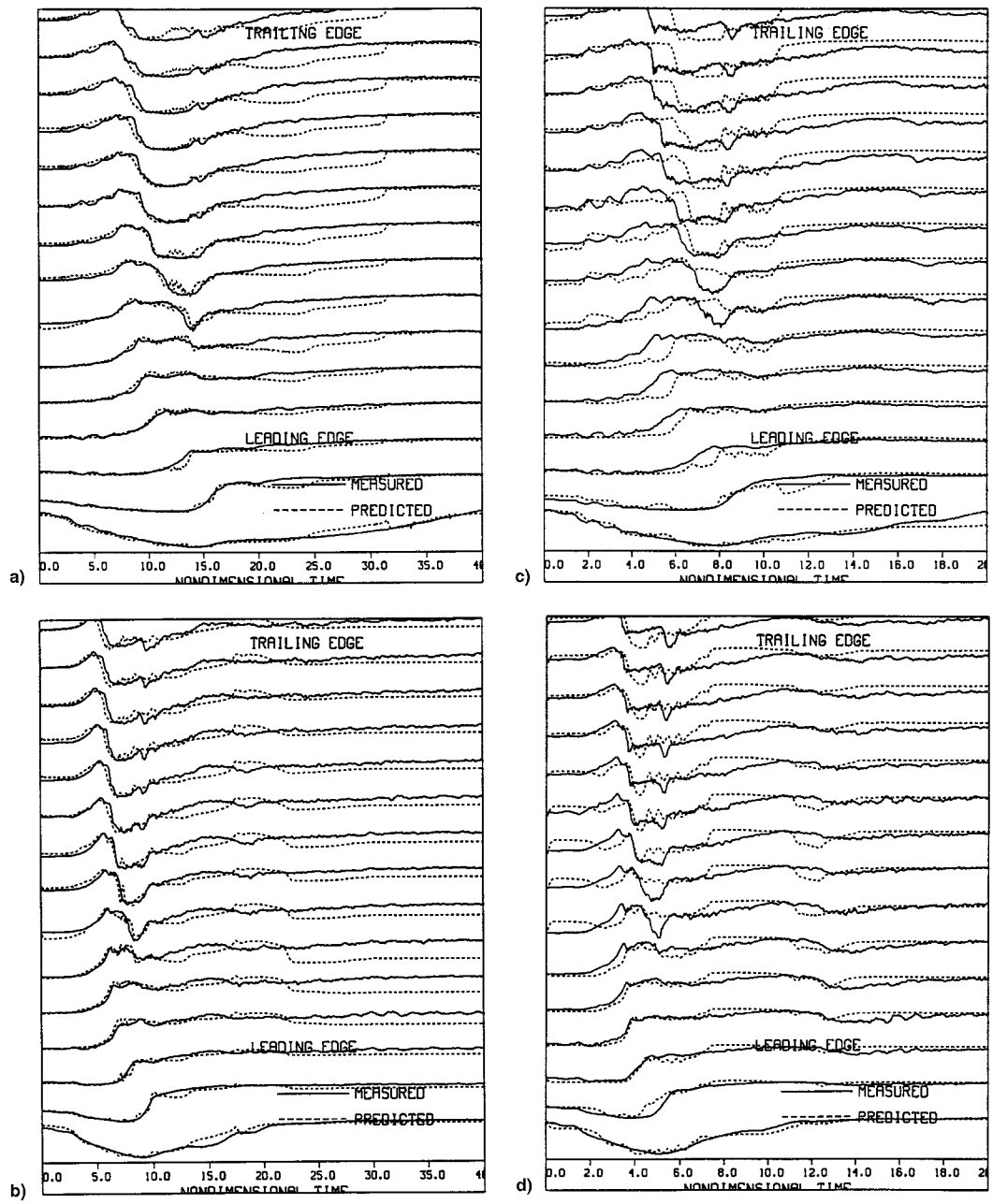

Fig. 7 RNN predictions for a shear-stress model trained on three of four test section velocities (Reynolds numbers 2.3×10^4, 4.6×10^4, and 1.84×10^5): a) predicted and measured shear-stress values for a pitch rate of 183 deg/s and Reynolds number 1.84×10^5, b) pitch rate of 367 deg/s and Reynolds number 1.84×10^5, c) pitch rate of 183 deg/s and Reynolds number 9.2×10^4, and d) pitch rate of 367 deg/s and Reynolds number 9.2×10^4.

shows similar results for a pitch rate on which the RNN model was not trained (367 deg/s). Again, events up to LEV passage are well predicted. However, the RNN-predicted values tend to lead the measurements. In general, as measured by the time-averaged error, the RNN shear-stress predictions were within 10% of the experimental values.

Figures 7a–7d show the results for the RNN model trained on three of four test section velocities and four of six pitch rates. Figure 7a shows the results for a pitch rate (183 deg/s) and Reynolds number (1.84×10^5) on which the model was trained. Shear-stress values were accurately predicted, however, following passage of the LEV the decrease in heat transfer was underpredicted. Figure 7b shows similar results for a Reynolds number of 1.84×10^5, and a pitch rate (367 deg/s) on which the model was not trained. In this case, predicted transition slightly leads the measurements. Consistent with previous results, the magnitude of the decrease in heat transfer following passage of the LEV was not accurately predicted.

Figures 7c and 7d show the results for a Reynolds number of 9.2×10^4, on which the RNN model was not trained. Figure 7c shows the results for a pitch rate of 183 deg/s. Initial shear-stress values are reasonably well predicted. However, boundary-layer transition significantly lags the measurements. Following LEV passage, the decrease in heat transfer is overpredicted. Figure 7d shows similar results for a pitch rate of 367 deg/s. In this case, predicted transition only slightly lags the measurement, but the decrease in heat transfer is not well predicted.

Although further work remains to be done, these results suggest that RNN models can accurately predict unsteady boundary-layer development and separation across a broad range of pitch rates and Reynolds numbers. Given the complexity of

the task, the quality of the predictions (10–20% error on average) was encouraging. Further, these results suggest that the capability to include freestream or test section velocities as inputs to the RNN models should extend to surface pressure measurements. Thus, using RNNs, it should be possible to model both unsteady boundary-layer behavior and the corresponding unsteady surface pressures across a wide range of pitch rates and Reynolds numbers.

Conclusions

The work described herein shows that RNNs can be used to accurately predict unsteady aerodynamics. Using RNNs, time-dependent models that predict unsteady boundary-layer development and separation, dynamic stall, and dynamic reattachment have been developed. RNN models can incorporate the widely differing physics of either the unsteady separating boundary layer, or of the globally separated unsteady flowfield dominated by a large energetic vortex. Operationally, the unsteady flowfield wing interactions could be defined for any time period over which the motion history was a known function (a few milliseconds to tens of seconds).

Overall, the results showed that given only limited training data, the following can be accomplished using RNNs.

1) RNN models can be developed that accurately predict the pressure distribution of three-dimensional unsteady separated flowfields for pitch-up wing motions.

2) RNN models can be developed that accurately predict the pressure distribution of three-dimensional dynamic reattachment for pitch-down wing motions.

3) RNN models can be developed that accurately predict the pressure distribution of three-dimensional unsteady separated flowfields for harmonic wing motions that give rise to both vortex absent and vortex present flowfields. Further, these models provided an indication that an accurate set of physical rules describing both types of flowfields can only be determined from a mix of vortex absent and vortex present records. As shown herein, this mix seems to be weighted toward the vortex present rules.

4) It appears that RNN models can be developed that accurately predict unsteady boundary-layer development and separation across a broad range of pitch rates and Reynolds numbers for a two-dimensional airfoil.

Further, as previously shown, these models of the flow–wing interactions can be used as the foundation for developing adaptive control systems.[22] Using an RNN model of the surface pressure topologies and aerodynamic coefficients, two approaches were shown for controlling the unsteady aerodynamic forces. First, a method for optimizing crucial parameters was explored. Second, a neural network controller was used to develop a real-time, closed-loop control system for commanding unsteady L/D. The results showed that neural network controllers provide one approach to the control of unsteady fluid mechanics problems. In the near future, such techniques will provide a viable approach for the development of six degree-of-freedom motion simulators for severe vehicle maneuvers as well as a foundation for the active control of unsteady fluid mechanics in a broad range of systems and devices.[25,26]

References

[1]Robinson, M., Walker, J., and Wissler, J., "Unsteady Surface Pressure Measurements on a Pitching Rectangular Wing," *Proceedings of Workshop II on Unsteady Separated Flow*, U.S. Air Force Academy, Colorado Springs, CO, 1988, pp. 225–237.

[2]Lorber, P., Covino, A., and Carta, F., "Dynamic Stall Experiments on a Swept Three-Dimensional Wing in Compressible Flow," AIAA Paper 91-1795, June 1991.

[3]Schreck, S., Addington, G., and Luttges, M., "Flow Field Structure and Development near the Root of a Straight Wing Pitching at Constant Rate," AIAA Paper 91-1793, June 1991.

[4]Schreck, S., and Helin, H., "Unsteady Vortex Dynamics and Surface Pressure Topologies on a Pitching Wing," *Journal of Aircraft*, Vol. 31, No. 4, 1994, pp. 899–907.

[5]Niven, A. J., Galbraith, R. A. M., and Herring, D. G. F., "Analysis of Reattachment During Ramp-Down Tests," *Vertica*, Vol. 13, No. 2, 1989, pp. 187–196.

[6]Niven, A. J., and Galbraith, R. A. M., "Experiments on the Establishment of Fully Attached Aerofoil Flow from the Fully Stalled Condition During Ramp-Down Motions," International Council of the Aeronautical Sciences, Paper 90-3.4.3, Sept. 1990.

[7]Ahmed, S., and Chandrasekhara, M. S., "Reattachment Studies of an Oscillating Airfoil Dynamic Stall Flow Field," AIAA Paper 91-3225, Sept. 1991.

[8]Schreck, S. J., and Faller, W. E., "Dynamic Reattachment on a Downward Pitching Finite Wing," AIAA Paper 94-3426, June 1994.

[9]Robinson, M., Galbraith, R., Shipley, D., and Miller, M., "Unsteady Aerodynamics of Wind Turbines," AIAA Paper 95-0526, Jan. 1995.

[10]Carr, L. W., "Progress in Analysis and Prediction of Dynamic Stall," *Journal of Aircraft*, Vol. 25, No. 1, 1988, pp. 6–17.

[11]Carr, L. W., and McCroskey, W. J., "A Review of Recent Advances in Computational and Experimental Analysis of Dynamic Stall," International Union of Theoretical and Applied Mechanics Symposium on Fluid Dynamics of High Angle of Attack, Tokyo, Japan, Sept. 1992.

[12]Knight, D., and Choudhuri, P., "2-D Unsteady Leading Edge Boundary Layer Reversal on a Pitching Airfoil," AIAA Paper 93-2977, July 1993.

[13]Sewall, W. G., Stack, J. P., McGhee, R. J., and Mangalam, S. M., "A New Multipoint Thin-Film Diagnostic Technique for Fluid Dynamic Studies," Society of Automotive Engineers Technical Paper Series, Anaheim, CA, Oct. 1988.

[14]Schreck, S. J., Faller, W. E., and Helin, H. E., "Pitch Rate and Reynolds Number Effects On Unsteady Boundary Layer Transition and Separation," AIAA Paper 94-2256, June 1994.

[15]Ericsson, L. E., "What About Transition Effects?," AIAA Paper 88-0564, Jan. 1988.

[16]Lorber, P., and Carta, F., "Unsteady Transition Measurements on a Pitching Three-Dimensional Wing," Fifth Symposium on Numerical and Physical Aspects of Aerodynamic Flows, California State Univ., Long Beach, CA, Jan. 1992.

[17]Wilder, M., Chandrasekhara, M., and Carr, L., "Transition Effects on Compressible Dynamic Stall of Transiently Pitching Airfoils," AIAA Paper 93-2978, July 1993.

[18]Carr, L., and Cebeci, T., "Boundary Layers on Oscillating Airfoils," Third Symposium on Numerical and Physical Aspects of Aerodynamic Flows, California State Univ., Long Beach, CA, Jan. 1985.

[19]Linse, D., and Stengel, R., "Identification of Aerodynamic Coefficients Using Computational Neural Networks," AIAA Paper 92-0172, Jan. 1992.

[20]Steck, J., and Rokhsaz, K., "Use of Neural Networks in Control of High Alpha Maneuvers," AIAA Paper 92-0048, Jan. 1992.

[21]Schreck, S. J., Faller, W. E., and Luttges, M. W., "Neural Network Prediction of Three-Dimensional Unsteady Separated Flowfields," *Journal of Aircraft*, Vol. 32, No. 1, 1995, pp. 178–185.

[22]Faller, W. E., Schreck, S. J., and Luttges, M. W., "Neural Network Prediction and Control of Three-Dimensional Unsteady Separated Flowfields," *Journal of Aircraft*, Vol. 32, No. 6, 1995, pp. 1213–1220.

[23]Faller, W. E., Schreck, S. J., and Helin, H. E., "Real-Time Model of Three-Dimensional Dynamic Reattachment Using Neural Networks," *Journal of Aircraft*, Vol. 32, No. 6, 1995, pp. 1177–1182.

[24]Jacobs, J. H., Hedgecock, C. E., Lichtenwalner, P. F., and Pado, L. E., "Use of Artificial Neural Networks for Buffet Environments," *Journal of Aircraft*, Vol. 31, No. 4, 1994, pp. 831–839.

[25]Faller, W. E., Smith, W. E., Nigon, R. T., and Huang, T. T., "Six Degree-of-Freedom Maneuvering Simulation of an Experimental Model Undergoing Severe Maneuvers Using Recursive Neural Networks," AIAA Paper 96-2492, June 1996.

[26]Faller, W. E., and Schreck, S. J., "Neural Networks: Applications and Opportunities in Aeronautics," *Progress in Aerospace Sciences*, Vol. 32, No. 5, 1996, pp. 433–456.